Characterization and Catalytic Performances of Three-Dimensional Mesoporous FeSBA-1 Catalysts

Ajayan Vinu,*,† Thangavelu Krithiga,‡ Veerappan Vaithilingam Balasubramanian,§ Anjana Asthana,⊥ Pavuluri Srinivasu,† Toshiyuki Mori,† Katsuhiko Ariga,† Ganapathiraman Ramanath,# and Pethuraja Gopal Ganesan‖

Nano-ionics Materials Group and Advanced Electron Microscopy Group, National Institute for Materials Science, 1–1, Namiki, Tsukuba, 305-0044, Japan, Department of Marine Biotechnology, Soonchunhyang University, Asan-City 336-745, Chungnam, South Korea, Department of Chemistry, Anna University, Chennai 600 025, India, Materials Science & Engineering Department and Center for Integrated Electronics, Rensselaer Polytechnic Institute, 110 eighth Street, Troy, New York 12180

Iron substituted cubic cage type mesoporous molecular sieves (FeSBA-1) were synthesized for the first time in a highly acidic media using cetyltriethylammonium bromide as a template. The amount of Fe incorporation in SBA-1 can easily be controlled by the simple adjustment of the molar hydrochloric acid-to-silicon ratio. All the materials were unambiguously characterized by AAS, XRD, N_2 adsorption, UV–Vis DRS, XPS, and ESR spectroscopy. The results from AAS, XRD, and N_2 adsorption reveal that the iron atom can be incorporated in the framework of SBA-1 matrix without altering the structural order and the textural parameters. The nature and the coordination of iron atoms were extensively studied by XPS spectroscopy, and the results revealed that most of the iron atoms in FeSBA-1 are in +3 coordination state. UV–Vis DRS and ESR studies confirmed that the majority of the Fe atoms in FeSBA-1 exist in a tetrahedral coordination environment (most probably occupying framework positions). *tert*-Butylation of phenol employing *tert*-butanol as the alkylation agent was carried out over FeSBA-1 catalysts with different iron content and the results are comapred with one-dimensional mesoporous catalysts. The influence of various reaction parameters such as reaction temperature, reactant feed ratio, weight hourly space velocity, and time-on-stream affecting the activity and selectivity of FeSBA-1 were also studied. Under the optimized reaction conditions, the FeSBA-1(36) catalyst showed superior catalytic performance for the *tert*-butylation of phenol as compared to the uni-dimensional mesoporous catalysts.

Introduction

Mesoporous molecular sieves have attracted considerable attention in recent years because of their excellent textural characteristics that made them effective biological adsorbents and catalysts in processes which allow easy diffusion of large-size organic molecules to internal active sites. These materials were first discovered by researchers of the Mobil Oil Corporation and named as M41S, a new family of mesoporous materials.[1] Originally, this family has been classified into three subgroups: a hexagonal (MCM-41), a cubic (MCM-48), and a lamellar phase (MCM-50). Among these novel materials, phases with a three-dimensional pore system are believed to be more advantageous for catalytic applications than phases having a one-dimensional array of pores. It is surmised that three-dimensional pore arrangements are more resistant to pore locking and allow faster diffusion of reactants. Surprisingly, the majority of studies published so far deal with phases having a one-dimensional pore system, viz. MCM-41 and SBA-15.[2–6]

Huo et al.[7–10] have synthesized a novel mesoporous molecular sieve with a three-dimensional cubic structure (space group *Pm3n*) of uniform pore size. The novel material, denoted SBA-1, has a cage-type structure with open windows,[11,12] and was formed by a $(S^+ \ X^- \ I^+)$ pathway (cationic surfactants (S^+), halogen anions (X^-) and cationic silicic acid species (I^+)). Tatsumi et al. have investigated the synthesis of V- and Mo-containing SBA-1[13] and gained control of the crystal morphology.[14] More recently, Vinu et al. have reported the direct synthesis of AlSBA-1 containing exclusively tetrahedrally coordinated aluminum and the catalytic activity of this material in the isomerization of *n*-decane,[15] as well as the synthesis of cobalt-containing SBA-1.[16]

Iron containing microporous molecular sieves have attracted considerable attention due to their remarkable activity as catalysts for the reduction of nitrous oxides,[17] oxidation of benzene to phenol[18] and the selective oxidation of methane.[19] However, they are not useful for treating heavier feeds and the production of more bulky fine chemicals, owing to their small pore size. Very recently, Vinu et al. have reported preliminary results on the direct synthesis and catalytic applications of FeSBA-1 mesoporous molecular sieves.[20] In our previous communication, we described a technique to incorporate Fe into SBA-1 by simply adjusting the molar hydrochloric acid-to-silicon ratio in the synthesis gel. In the present contribution, much emphasis has been given to the material characterizations,

* To whom correspondence should be addressed. Phone: +81-29-860-4563. Fax: +81-29-860-4667. E-mail: vinu.ajayan@nims.go.jp.
† Nano-ionics Materials Group, National Institute for Materials Science.
⊥ Advanced Electron Microscopy Group, National Institute for Materials Science.
§ Department of Marine Biotechnology, Soonchunhyang University.
‡ Department of Chemistry, Anna University.
# Materials Science & Engineering Department.
‖ Center for Integrated Electronics, Rensselaer Polytechnic Institute.

Three-Dimensional Mesoporous FeSBA-1 Catalysts

J. Phys. Chem. B, Vol. 110, No. 24, 2006 **11925**

especially by XPS spectroscopy and nitrogen adsorption and in-depth study on their catalytic performances in the *tert*-butylation of phenol.

Alkylation of phenol is an industrially important reaction because many alkylphenols are used as intermediates in the manufacture of antioxidants, ultraviolet absorbers, phenolic resins, polymerization inhibitors, and heat stabilizers.[21] 4-*tert*-Butylphenol (4-TBP) imparts improved performance properties to the class of metallic detergents (phenates) used in lubricating oils. *tert*-Butylation of phenol has been extensively studied using aluminum chloride, phosphoric acid, sulfuric acid, silica−alumina, cation-exchange resins, and microporous molecular sieves.[22,23] The major drawbacks of homogeneous catalysts are their hazardous nature and separation of the catalysts from the reaction mixture. The cationic exchange resins are not employed due to its lower stability at high temperature as well as lower activity and selectivity.[23] Much attention was given to molecular sieves due to their activity, selectivity, and reusability.[24,25] Zhang et al.[26] studied the *tert*-butylation of phenol with *tert*-butanol over zeolite H-β and found that strong acid sites are helpful for the formation of 2,4-di-*tert*-butylphenol (2−4DTBP) and medium acid sites are advantageous to produce *p*-isomer (4-TBP), while weak acid sites are effective in producing the *o*-isomers. It has been proposed that activity and selectivity of catalysts depend on the nature of acid sites present in the catalyst. Recently Selvam and co-workers have reported the *tert*-butylation of phenol over mono-metal substituted AlMCM-41 or FeMCM-41 and proposed that the moderate acidity of these catalysts is favorable for formation of 4-*tert*-butylphenol.[27] FeSBA-1 catalysts are very active and are expected to give significantly higher conversions of phenol and selectivity to 4-*tert*-butylphenol when compared to mono- and bimetal substituted uni-dimensional MCM-41 materials.

Experimental Section

Iron containing SBA-1 was synthesized under acidic conditions using cetyltriethylammonium bromide (CTEABr) as the surfactant, tetraethyl orthosilicate (TEOS) as the silica source, and ferric nitrate nonahydrate as the iron source. The surfactant (CTEABr) was synthesized by reaction of 1-bromohexadecane with an equimolar amount of triethylamine in ethanol under reflux conditions for 2 days. The resulting solid CTEABr was purified by recrystallization from a chloroform/ethyl acetate mixture. A typical synthesis procedure for FeSBA-1 is as follows: Solution A was prepared by adding 0.812 g of CTEABr to an appropriate amount of the aqueous solution of 4.4M HCl (n_{HCl}/n_{H_2O} ratio was fixed to 0.08). The solution thus obtained was cooled to 0 °C and homogenized for 30 min. TEOS and Fe(NO$_3$)$_3$ · 9 H$_2$O were precooled to 0 °C and then added to solution A under vigorous stirring, and we continued the stirring for another 5 h at 0 °C. Thereafter, the reaction mixture was heated to 100 °C for 1 h. A first set of samples was prepared by changing the molar HCl-to-silicon ratio and denoted as FeSBA-1(*x*H) where *x* denotes the molar molar HCl-to-silicon ratio (n_{HCl}/n_{Si}). A second set of samples was prepared by changing the n_{Si}/n_{Fe} ratio in the gel, and the n_{HCl}/n_{Si} ratio was fixed to 10. The samples were labeled FeSBA-1(*x*) where *x* denotes the n_{Si}/n_{Fe} molar ratio. The solid product was recovered by filtration and dried in an oven at 100 °C overnight. The molar composition of the gel was 1 TEOS: 0.0025−0.025 Fe$_2$O$_3$: 0.2 CTEABr: 10−56 HCl: 125−700 H$_2$O. The as-synthesized material was then calcined in air by raising the temperature from 20 to 550 °C with a heating rate of 1.8 °C/min and keeping the sample at the final temperature for 10 h.

Characterization. The powder X-ray diffraction patterns of FeSBA-1 materials were collected on a Siemens D5005 diffractometer using CuKα (λ = 0.154 nm) radiation. The diffractograms were recorded in the 2θ range of 0.8−10° with a 2θ step size of 0.01 ° and a step time of 10 s. Nitrogen adsorption and desorption isotherms were measured at −196 °C on a Quantachrome Autosorb 1 sorption analyzer. All samples were outgassed for 3 h at 250 °C under vacuum (p < 10^{-5} hPa) in the degas port of the adsorption analyzer. The specific surface area was calculated using the BET model. The pore size distributions were obtained from the adsorption and desorption branch of the nitrogen isotherms using the corrected form of the Kelvin equation by means of the Barrett−Joyner−Halenda method as proposed by Kruk et al.[28]

$$r(p/p_0) = 2\gamma V_L/RT\ln[p_0/p] + t(p/p_0) + 0.3 \text{ nm} \qquad (1)$$

In eq 1, V_L is the molar volume of the liquid adsorbate, γ is its surface tension (8.88·10^{-3} N/m), R is the gas constant (8.314 J/(mol·K)), and T is the absolute temperature (77 K). $t(p/p_0)$ is the statistical film thickness of nitrogen adsorbate in pores of the SBA-1 as a function of the relative pressure p/p$_0$).

UV−Vis diffuse reflectance spectra were measured with a Perkin-Elmer Lambda 18 spectrometer equipped with a Praying−Mantis diffuse reflectance attachment. BaSO$_4$ was used as reference. Elementary analysis was done using an Analyst AA 300 spectrometer. X-band EPR (9.7 GHz) spectra were recorded at −196 °C using a BRUKER ESP 300E spectrometer. X-ray photoelectron spectroscopy (XPS) measurements were carried out in a PHI 5400 instrument with a 200 W MgK-alpha probe beam to characterize the samples. The spectrometer was configured to operate at high resolution with pass energy of 20 eV. Prior to the analysis, the samples were evacuated at high vacuum and then introduced into the analysis chamber. Survey and multiregion spectra were recorded at O$_{1S}$, Si$_{2P}$, and Fe$_{2P}$ photoelectron peaks. Each spectra region of photoelectron interest was scanned several times to obtain good signal-to-noise ratios.

The *tert*-butylation of phenol was carried out in a fixed-bed flow-type reactor made up of a borosil glass tube with a length of 40 cm and an internal diameter of 2 cm. About 0.5 g of catalyst was placed in the reactor and supported on either side with a thin layer of quartz wool and ceramic beds. The reactor was heated to the reaction temperature with the help of a tubular furnace controlled by a digital temperature controller. The catalyst was activated in air at 550 °C for 6 h prior to the catalytic runs. Reactants were fed into the reactor using a syringe infusion pump. The bottom of the reactor was connected to a coiled condenser and receiver to collect the products. The products obtained in the first 20 min were discarded and the product collected after 1 h was analyzed for identification. The liquid products were analyzed by a Shimadzu gas chromatograph GC-17A using a DB-5 capillary column. Product identification was achieved by co-injection and GC−MS.

Results and Discussion

The n$_{Si}$/n$_{Fe}$ molar ratios of all FeSBA-1 samples prepared using different molar hydrochloric acid to silica (n$_{HCl}$/n$_{Si}$) ratios are summarized in Table 1 where the amount of Fe incorporation in SBA-1 is significantly increased with decreasing the n$_{HCl}$/n$_{Si}$ ratio from 56 to 10. The higher amount of iron atom incorporation at a lower n$_{HCl}$/n$_{Si}$ ratio in SBA-1 can be explained by the surfactant silica assembly mechanism: The formation of the silica−surfactant mesophase under strongly acidic conditions

TABLE 1: Textural Parameters of FeSBA-1 Samples Prepared at Different n_{HCl}/n_{Si} and n_{Si}/n_{Fe} Ratios

catalysts	n_{Si}/n_{Fe} gel	product	n_{HCl}/n_{Si}	a_o (nm)	A_{BET} (± 5 m^2/g)	d_p, BJH (nm)	V_p, (cm^3/g)
FeSBA-1(56H)	20	315	56	7.8	1350	2.4	0.71
FeSBA-1(42H)	20	217	42	7.8	1290	2.4	0.71
FeSBA-1(28H)	20	86	28	7.7	1340	2.4	0.71
FeSBA-1(36) or FeSBA-1(10H)	20	36	10	7.9	1280	2.5	0.69
FeSBA-1(90)	40	90	10	7.8	1350	2.4	0.71
FeSBA-1(120)	67	120	10	7.6	1390	2.4	0.70
FeSBA-1(344)	200	344	10	7.5	1380	2.3	0.66
FeMCM-41	20	23	-	4.10	770	2.5	0.50

occurs through the formation of S$^+$X$^-$I$^+$ micelles (S$^+$ denotes surfactant cation, X$^-$ the halogen anion, and I$^+$ the protonated inorganic SiO$_2$ species). Since the I$^+$ species are positively charged by protonation at low pH, the interaction of the surfactant S$^+$ with the I$^+$ species occurs via a SiO$_2$/H$^+$/X$^-$/CTEA$^+$ bridge, where the protonated silica surface is linked to the cationic surfactant headgroup via a halogen anion. At a lower n_{HCl}/n_{Si} ratio, the reduced positive charge on the silica could enhance the interaction between the silica species and iron hydroxo complexes (Fe (OH)$_2^+$), resulting in a higher amount of Fe incorporation in the cubic SBA-1 silica matrix. It is also interesting to note that the amount of Fe incorporation increases with increasing metal content in the synthesis gel. As shown in Table 1, the amount of iron incorporated into the solid is lower than in the input gel composition probably due to the higher solubility of the iron source in highly acidic synthesis medium.
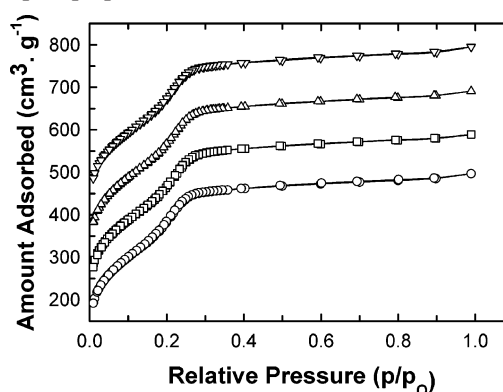
Figure 1 shows the powder XRD patterns of FeSBA-1 samples prepared using different n_{HCl}/n_{Si} ratios at a constant input n_{Si}/n_{Fe} gel ratio of 20. All the samples exhibit an intense (210) reflection and smaller (200) and (211) reflections. This characteristic XRD patterns of the SBA-1 cubic phase, which can be indexed to *Pm3n* space group, matches well with those reported in the literature.[7−10] However, the decrease in intensity of the (200) and (211) reflections, with a decreasing n_{HCl}/n_{Si} ratio, suggests that the higher amount of iron incorporation in the mesoporous materials might reduce the degree of ferro-silicate polymerization accompanied by a slight change in structural order (during calcination). Upon calcination of the as-synthesized materials, the XRD patterns of FeSBA-1 become better resolved and the intensity of the XRD patterns increases significantly as a result of the removal of the intercalated organic template. These results indicate that the amount of iron in the SBA-1 materials can easily be controlled by the simple adjustment of the n_{HCl}/n_{Si} ratio without affecting the structural order of SBA-1 materials.

The powder XRD pattern of FeSBA-1 samples prepared at a different n_{Si}/n_{Fe} ratio is also shown in Figure 1. All the samples
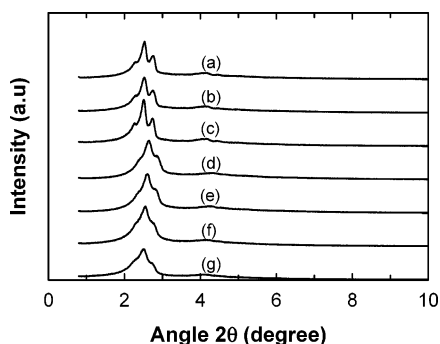
display an intense (210) reflection and smaller (200) and (211) reflections. It is interesting to note that the intensity of the (210) peak increase with increasing Fe content of the material. The observed *d* spacings are compatible with the cubic *Pm3n* space group. The unit cell parameter was calculated using the following equation: $a_0 = d_{210} \sqrt{5}$. The unit cell parameter is increased from 7.5 to 7.9 nm with increasing Fe content (Table 1). A similar result has also been observed in V−SBA-1 molecular sieves.[13]

Information on the textural properties of porous solids are typically obtained from low-temperature (−196 °C) nitrogen adsorption isotherms, which allow calculation of the specific surface area, specific pore volume, and mesopore size distribution. The nitrogen adsorption−desorption isotherms of the FeSBA-1 samples prepared at a different n_{HCl}/n_{Si} ratio are shown in Figure 2, and the textural properties are collected in Table 1. All isotherms are of type IV according to the IUPAC classification and exhibited no hysteresis loop. It is interesting that the capillary condensation step is relatively broad (p/p$_0$ = 0.15−0.25) as compared to MCM-41 or MCM-48 despite the high periodicity of the SBA-1 structure as evident from the corresponding XRD pattern. This result has been ascribed to the peculiarity of the SBA-1 structure consisting of two types of cage-like pores. It is important to note that the shape and type of the isotherms of FeSBA-1 materials prepared at a different n_{HCl}/n_{Si} ratio are similar to that of well ordered cubic mesoporous SBA-1 silica materials as reported by Huo et al.,[10] suggesting that the cubic cage type structure is preserved in the FeSBA-1 materials and controlling the amount of metal ion incorporation by changing the n_{HCl}/n_{Si} is the best approach to prepare metal substituted SBA-1 materials. The textural parameters such as specific surface area, specific pore volume, and the pore diameter of the FeSBA-1 samples prepared at a different n_{HCl}/n_{Si} ratio are given in Table 1. As can be seen in Table 1, only a slight change in the textural parameters is observed for the samples prepared at a different n_{HCl}/n_{Si} ratio.

Figure 1. XRD powder patterns of calcined FeSBA-1 samples: (a) FeSBA-1(56H), (b) FeSBA-1(42H), (c) FeSBA-1(28H), (d) FeSBA-1(344), (e) FeSBA-1(120), (f) FeSBA-1(90), and (g) FeSBA-1(36).

Figure 2. Nitrogen adsorption isotherms of FeSBA-1 materials prepared at different n_{HCl}/n_{Si} ratios: (●) FeSBA-1(56H), (■) FeSBA-1(42H), (▲) FeSBA-1(28H), and (◆) FeSBA-1(10H).

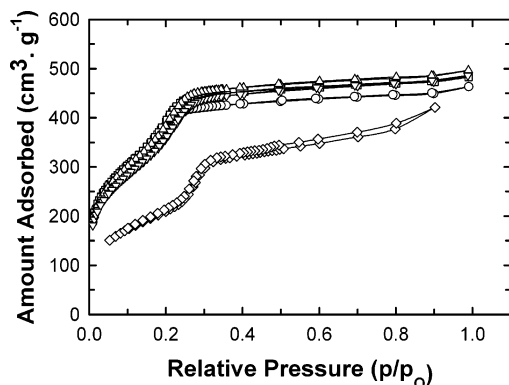Three-Dimensional Mesoporous FeSBA-1 Catalysts

J. Phys. Chem. B, Vol. 110, No. 24, 2006 **11927**

Figure 3. Nitrogen adsorption isotherm of FeSBA-1 materials prepared at different n_{Si}/n_{Fe} ratios: (○) FeSBA-1(344), (□) FeSBA-1(120) and (△) FeSBA-1(90), (▽) FeSBA-1(36), and (◇) FeMCM-41(23).
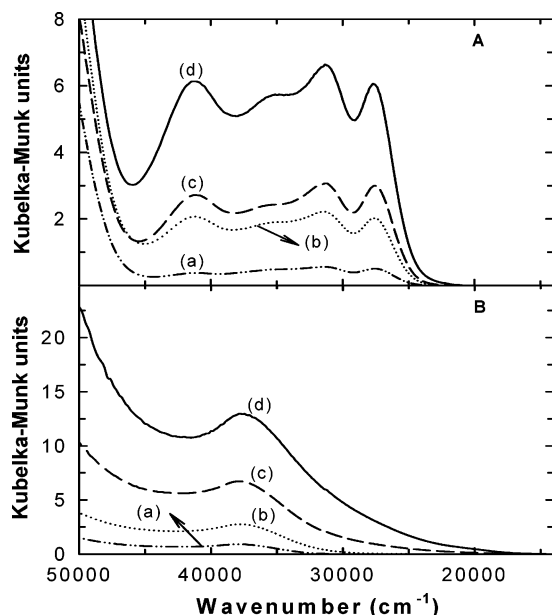

Figure 4. UV−Vis DRS spectra of (A) as-synthesized and (B) calcined FeSBA-1 samples with different n_{Si}/n_{Fe} ratio: (a) FeSBA-1(344), (b) FeSBA-1(120), (c) FeSBA-1(90), and (d) FeSBA-1(36).

Figure 3 shows the nitrogen adsorption isotherms of FeSBA-1 samples synthesized with different n_{Si}/n_{Fe} ratios. All isotherms show a slightly broad condensation step at relative pressures in the range of 0.1−0.3. The textural parameters of the corresponding samples are also given in the Table 1. The specific surface area decreases from 1385 m^2/g for FeSBA-1(344) to 1275 m^2/g for FeSBA-1(36) whereas the pore diameter calculated from the adsorption branch of the isotherm increases from 2.3 for FeSBA-1(344) to 2.5 nm for FeSBA-1(36). Moreover, the specific pore volume increases from 0.66 cm^3/g to 0.71 cm^3/g up to a n_{Si}/n_{Fe} ratio of 90, and then decreases to 0.69 cm^3/g for a n_{Si}/n_{Fe} ratio of 36. The increase in pore diameter of FeSBA-1 with increasing Fe content indicates that Fe atoms are occupying framework positions in SBA-1. Moreover, the high specific surface area and pore volume even at high Fe loading indicate that high quality FeSBA-1 can be obtained. It is important to note that specific surface area and pore volume of FeMCM-41 are lower as compared to FeSBA-1 samples (Table 1).

Figure 4 displays the UV−Visible DRS spectra of as-synthesized FeSBA-1 with a different n_{Si}/n_{Fe} ratio. All the spectra consist of four components with maxima at 41 666, 35 714, 31 545, and 27 777 cm^{-1}. The intensity of all peaks is
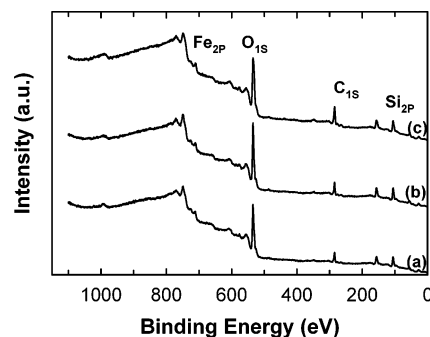

Figure 5. The XPS survey spectrum of FeSBA-1 samples with different n_{Si}/n_{Fe} ratio: (a) FeSBA-1(36), (b) FeSBA-1(90), and (c) FeSBA-1(120).

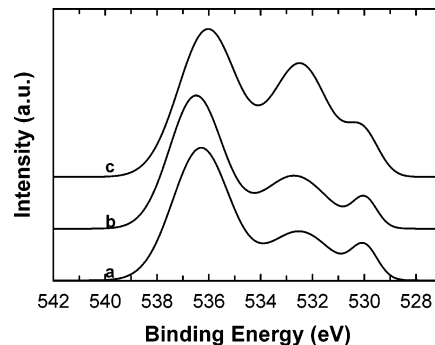**Figure 6.** O$_{1S}$ core-level spectra of FeSBA-1 samples with different n_{Si}/n_{Fe} ratio: (a) FeSBA-1(120), (b) FeSBA-1(90), and (c) FeSBA-1(36).

rising with increasing iron loading. The bands near 41 666, 35 714, and 31 545 cm^{-1} can be unambiguously assigned to the Laporte-allowed ligand-to-metal electron transition consistent with tetrahedral sites in agreement with previous studies on FePO$_4$, Fe−HMS, and FeS-1 silicalites.[29] Moreover, the band near 27 777 cm^{-1} is seen in all materials except the one with the very low Fe content. This band could be attributed to $^6A_1 \rightarrow {}^4E$ energy transition, which is a strong indication for tetrahedral coordination of Fe species. Upon calcination, the entire absorption band has been merged together to a single absorption band near 37 735 cm^{-1}, which is attributed to tetrahedrally coordinated iron species. A similar band was also reported in ferrisilicate materials containing tetrahedrally coordinated iron species.[30] This indicates that iron still exists in the tetrahedral coordination even after calcination. However, for the FeSBA-1(36) sample, a change in color is observed. Moreover, a broad absorption band in the visible region is detected, probably due to the presence of Fe(II) or Fe$_2$O$_3$ species.[29] The information collected so far supports the assumption that the majority of the iron atom exists in tetrahedral coordination in SBA-1 framework.

XPS was used to analyze the nature and coordination of the elements present in FeSBA-1 samples using their respective binding energy values. Figure 5 shows the survey spectrum of FeSBA-1 samples with different n_{Si}/n_{Fe} ratios. All the samples exhibit five sharp peaks which are attributed to Fe$_{2P}$, O$_{1S}$, C1S, Si2S, and Si$_{2P}$. The C1S peak can be assigned to the adventitious carbon for calibrating binding energy as a reference. The elemental composition of, mainly, Si and Fe of all the samples from their survey spectrum is in close agreement with the results obtained from the elementary analysis.

Figure 6 shows the O$_{1S}$ spectra of FeSBA-1 samples with a different n_{Si}/n_{Fe} ratio. The O$_{1S}$ spectra are similar in shape for all the samples, showing three well-defined peaks with binding

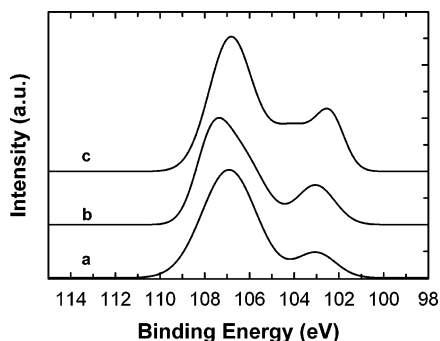**11928** *J. Phys. Chem. B, Vol. 110, No. 24, 2006*

Vinu et al.

Figure 7. Si_{2P} core-level spectra of FeSBA-1 samples with different n_{Si}/n_{Fe} ratio: (a) FeSBA-1(120), (b) FeSBA-1(90), and (c) FeSBA-1(36).

Figure 8. Fe_{2P} core-level spectra of FeSBA-1 samples with different n_{Si}/n_{Fe} ratio: (a) FeSBA-1(120), (b) FeSBA-1(90), and (c) FeSBA-1(36).

energy values of 530.0, 532.4−532.7, and 536−536.3 eV. This indicates that three different kinds of oxygen environment are present in the surface of all samples. The binding energy values of the three types of O_{1S} can easily be judged from the difference in the electronegativity of the elements. The O_{1S} peak at 530.0 eV can be assigned to oxygen atoms coordinated to the Fe metal cations. It is interesting to note that the intensity of the peak increases with increasing the iron content in the samples. It implies that the number of Fe−O−Fe groups on the surface of the samples increases with increasing the iron content. The O_{1S} peak at 532.4−532.7 eV can be assigned to both Si−O−Si and Si−O−Fe. The intensity of the O_{1S} peak corresponding to the Si−O−Si and Si−O−Fe were significantly increased when the amount of iron content increased in SBA-1 matrix. Moreover, the values of the binding energy for the O_{1S} peak was shifted from higher (532.7 eV) to lower value (532.4 eV). The change in the intensity of the peak and the shifting behavior O_{1S} can be explained as follows: As the amount of Fe increases in the sample, some of the silicon atoms in the Si−O−Si groups of the FeSBA-1 are replaced by the Fe atoms, resulting in the increase of Si−O−Fe groups. The change in the number of Si−O-Me is solely responsible for the shift in the binding energy. This also indicates that the FeSBA-1(36) sample contains a higher number of Si−O−Fe groups on the surface and Fe is well incorporated inside the framework. The O_{1S} peak at 536.0 to 536.3 eV is mainly associated with the water molecules coordinated either to the iron or silicon atoms. Similar results have also been reported in the metal substituted aerogels.[31]

Figure 7 shows the Si_{2P} region of FeSBA-1 samples with different n_{Si}/n_{Fe} ratio. All the samples have two components at 102.6−103.0 and 106.9 eV. It can be seen from Figure 7 that the intensity of the Si_{2P} peak increases with increasing the iron content in the samples. Moreover, the value of the binding energy of the Si_{2P} peak decreased from 103.0 to 102.6 eV with an increase of iron content in the sample. The Si_{2P} peak at 103 eV is assigned to Si−O−Si, while the peak at 102.6 eV can be assigned to Si−O-Me.[32] The main reason for the shifting in the binding energy upon iron loading is the difference in the electronegativity of Fe and Si. The low electron affinity of iron causes movement of electrons from iron to silicon and then a decrease in the binding energy of Si_{2P}. This reveals that a greater number of Fe atoms are surrounded by the silicon atoms in the sample having very high iron content, namely FeSBA-1(36), most likely in the structure of Si−O−Fe. These results also confirmed the partial change in the framework structure from pure silicate to ferrosilicates.

The Fe_{2P} spectra of the FeSBA-1 sample with different iron content are shown in Figure 8. As can be seen in the Figure 8, all the samples had two sharp peaks with binding energy values
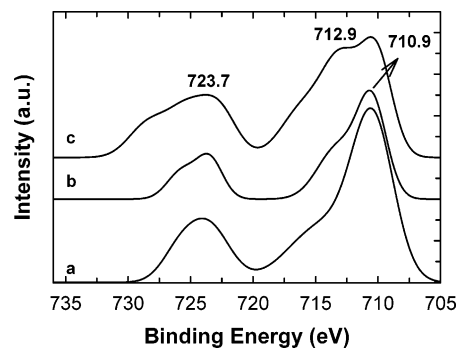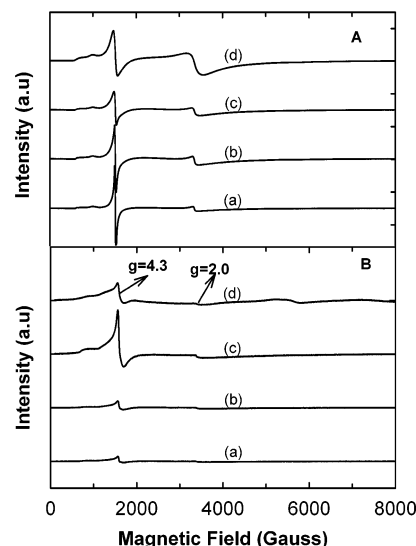

Figure 9. ESR spectra of (A) as-synthesized and (B) calcined FeSBA-1 samples with different n_{Si}/n_{Fe} ratios: (a) FeSBA-1(344), (b) FeSBA-1(120), (c) FeSBA-1(90), and (d) FeSBA-1(36).

of 710.9 and 723.7 eV. In the case of FeSBA-1(36), a shoulder peak with the binding energy of 712.9 eV was observed. The Fe_{2P} peak at 710.0 eV is typically assigned for iron atom with +3 coordination state. Similar results have also been reported in the iron substituted mesoporous silica materials.[33] Further, the shoulder peak in the FeSBA-1(36) at 712.9 eV can be assigned to small iron oxide particles which normally have binding energy values of 710.7 and 712 eV.[34] This reveals that the FeSBA-1(36) sample contain a little amount of octahedral coordinated iron atoms. In addition, the broad peak, which is centered at 723.7 eV, may be assigned to iron atoms coordinated to hydroxyl groups or water molecules in the samples.

The ESR spectra of the as-synthesized FeSBA-1 samples with different n_{Si}/n_{Fe} are shown in Figure 9. All the samples show two major components at $g = 4.3$ and 2.0, which rise in intensity with increasing n_{Si}/n_{Fe} ratio from 344 to 36. Similar spectra were previously found in Fe−HMS mesoporous materials by Tuel et al.[35] who suggested that the ESR signal at $g = 4.3$ corresponds to the strongly rhombic distorted $[FeO_4]^-$ tetrahedra and is originating from the lowest Kramers doublet and the middle Kramers doublet, respectively.[36] According to arguments by Goldfarb et al.,[36] the signal at $g = 2$ (Figure 9) clearly indicates the presence of tetrahedrally coordinated Fe^{3+} in all our samples.

The signal at $g = 4.3$ can be assigned to Fe framework ''defect'' sites with terminal oxygens.[36] There is a significant change in the X-band EPR spectrum of the calcined FeSBA-1 samples (Figure 9). The intensity of the signal at $g = 2$ is
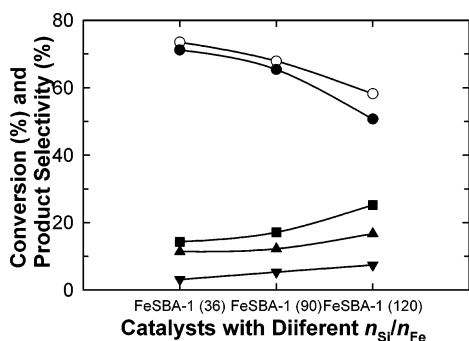
Three-Dimensional Mesoporous FeSBA-1 Catalysts

J. Phys. Chem. B, Vol. 110, No. 24, 2006 **11929**

Figure 10. Effect of the catalyst with different n_{Si}/n_{Fe} ratio on the phenol conversion and selectivity of products over FeSBA-1 catalyst with different n_{Si}/n_{Fe} at the WHSV of 4.86 h^{-1}, $n_{TBA}/n_{phenol} = 3$; (○) X_{Phenol}, (●) S_{4-TBP}, (■) S_{2-TBP}, (▲) $S_{2,4-DTBP}$, and (▼) S_{others}.

Figure 11. Effect of reaction temperature on the phenol conversion and selectivity of products over FeSBA-1(36) at the WHSV of 4.86 h^{-1}, $n_{TBA}/n_{phenol} = 3$; (○) X_{Phenol}, (●) S_{4-TBP}, (■) S_{2-TBP}, (▲) $S_{2,4-DTBP}$, and (▼) S_{others}.

drastically decreased after calcination, whereas the intensity of the signal at $g = 4.3$ increases. Moreover, the intensity of both signals increases with increasing Fe content. The absence of a signal at $g = 2.2$ in the calcined sample, which is normally assigned for an octahedral coordinated Fe atom, indicates that the Fe atoms are exclusively in tetrahedral coordination in the SBA-1 framework.

The *tert*-butylation of phenol using *tert*-butanol (TBA) was carried out over FeSBA-1 catalysts with different n_{Si}/n_{Fe} ratios (36, 90, and 120) at a reaction temperature of 200 °C, a WHSV of 4.86 h^{-1}, and n_{TBA}/n_{phenol} ratio of 3. The products obtained are 2-*tert*-butylphenol (2-TBP), 4-*tert*-butylphenol (4-TBP), and 2,4-di-*tert*-butylphenol (2,4-DTBP). Only traces of tri-*tert*-butylphenol and 3-*tert*-butylphenol were observed. Moreover, minor amounts of isobutene and its dimmers are formed. Phenol conversion and product selectivity over FeSBA-1 catalysts with different n_{Si}/n_{Fe} is presented in Figure 10. Phenol conversion and 4-TBP selectivity were found to be higher for FeSBA-1 (36) catalyst than other catalysts (Table 2). With increasing n_{Si}/n_{Fe} ratio, the activity of the catalysts increases also. A maximum phenol conversion of 78.5% was observed for the FeSBA-1(36) catalyst at a reaction temperature of 200 °C. The change in the selectivity of the products with increasing the n_{Si}/n_{Fe} is mainly due to the difference in the acid strength and the number of acid sites. It has been found that the activity of the catalysts changes in the following order: FeSBA-1(36) > FeSBA-1(90) > FeSBA-1(120). FeSBA-1(36) exhibits the best performance with a phenol conversion of 78.5% and 4-TBP yield of 55.9%, which are significantly higher as compared to other mono- and/or bimetal substituted uni-dimensional mesoporous materials such as H−AlMCM-41 and FeAlMCM-41 under optimized reaction conditions.[27,37] It should be noted that the uni-dimensional FeMCM-41(50) catalyst showed a phenol conversion of only 21.1% and a 4-TBP yield of 18.35% under comparable reaction conditions (Table 2). The observed higher
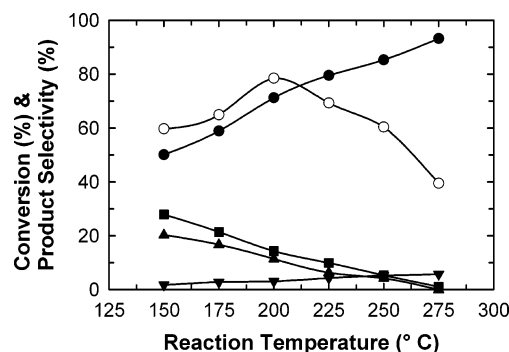
activity of FeSBA-1(36) is tentatively ascribed to its three-dimensional cage-type pore structure resulting in a higher number of accessible active sites and excellent textural parameters such as very high surface area and pore volume. As FeSBA-1(36) is the most active catalyst in this work we have chosen this catalyst for the more detailed study.

The effect of reaction temperature on the phenol conversion and product selectivity over FeSBA-1(36) at a WHSV of 4.86 h^{-1} and n_{TBA}/n_{phenol} ratio of 3 is shown in Figure 11. The phenol conversion steadily increases with increasing reaction temperature up to 200 °C. A further increase of the reaction temperature from 200 to 275 °C leads to a drastic reduction in the phenol conversion from 78.5 to 39.5%. The low conversion at high temperature may be due to the predominant dealkylation over alkylation at high temperature and also due to the diminishing availability of TBA as it undergoes side reactions such as oligomerization or aromatization.[26]

With increasing reaction temperature, the selectivity to 4-TBP rises and reaches a maximum of 93.2% at a reaction temperature of 275 °C. The observed increase in *p*-selectivity with increasing reaction temperature has been reported for other catalysts and explained by the different diffusion kinetics of 4-TBP as compared to the other products and absence of secondary alkylation.[37−39] Recently, Song et al.[39] have reported the preferential formation of *p*- isomers due to their different diffusional kinetics via computational modeling. Moreover it must be noted that the selectivity for 2,4-DTBP and 2-TBP is higher at lower reaction temperature and decreases with an increase in the reaction temperature. This may be due to the higher stability and the availability of *tert*-butyl cation at low reaction temperature. Moreover the formation of 4-TBP is thermodynamically favored at higher reaction temperature.

The effect of WHSV on alkylation of phenol with TBA over FeSBA-1(36) at a reaction temperature of 200 °C and n_{TBA}/

TABLE 2: Comparison of Phenol Conversion and Product Selectivity over FeSBA-1(36) with Other Catalysts Such as FeMCM-41(50), AlMCM-41(56), FeAlMCM-41(50), and Sulfated Zirconia under Comparable Reaction Conditions (Time-on-stream = 1 h)

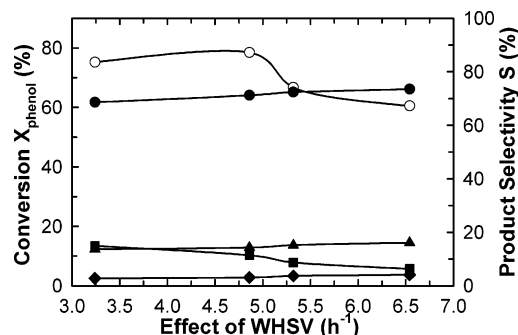|	FeSBA-1(36) this work	FeAlMCM-41 (20) ref 37	AlMCM-41 (56) ref 27	FeMCM-41 (50) ref 27	sulfated zirconia ref 2
$n_{t-butanol}/n_{phenol}$	3	3	2	2	2
WHSV/h^{-1}	4.86	5.12	4.8	4.8	5.2
reaction temp./°C	200	200	175	175	175
phenol conversion/%	78.5	70.1	35.9	21.1	57.8
selectivity/%					
2-TBP	14.3	10.4	8.1	9.5	6.8
3-TBP			4.7		
4-TBP	71.2	75.2	83.4	87	86.5
2,4-TBP	11.4	14.4	3.9	3.5	6.7

11930 *J. Phys. Chem. B, Vol. 110, No. 24, 2006*

Vinu et al.

Figure 12. Effect of WHSV on phenol conversion and products selectivity over FeSBA-1(36) catalyst (T_R = 200 °C, n_{TBA}/n_{phenol} = 3); (○) X_{Phenol}, (●) S_{4-TBP}, (■) S_{2-TBP}, (▲) $S_{2,4-DTBP}$, and (◆) S_{others}.

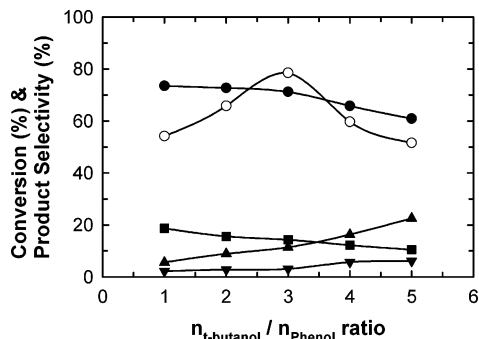**Figure 13.** Effect of n_{TBA}/n_{phenol} ratio on the activity and selectivity of FeSBA-1(36) (T_R = 200 °C, WHSV = 4.86 h^{-1}); (○) X_{Phenol}, (●) S_{4-TBP}, (■) S_{2-TBP}, (▲) $S_{2,4-DTBP}$, and (▼) S_{others}.
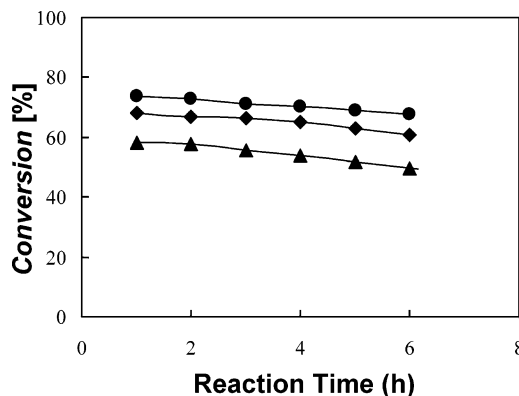

Figure 14. Effect of time on stream on phenol conversion over various FeSBA-1 catalysts at 200 °C: (●) FeSBA-1(36), (◆) FeSBA-1(90), and (▲) FeSBA-1(120).
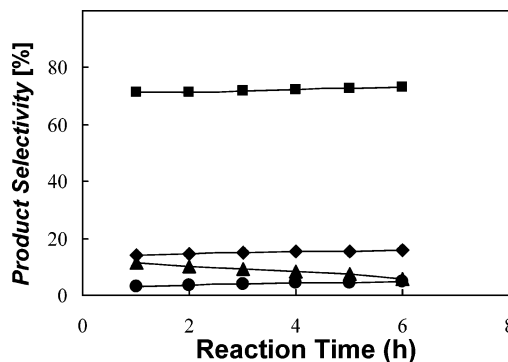

Figure 15. Effect of time on stream on the product selectivity over FeSBA-1(36) catalyst at 200 °C: (■) S_{4-TBP}, (◆) S_{2-TBP}, (▲) $S_{2,4-DTBP}$, and (●) S_{Others}.

n_{phenol} ratio of 1:3 was also investigated. Conversion and product selectivity of the reaction at different WHSV (3.24, 4.86, 5.32 and 6.54 h^{-1}) are shown in Figure 12. A slight increase in phenol conversion was observed when the WHSV was increased from 3.24 to 4.86 h^{-1}. Further increase in WHSV drastically decreased the phenol conversion. The reduction in conversion at higher WHSV may be simply due to shorter contact time at higher space velocity. The selectivity of 4-TBP and 2-TBP is found to decrease with decrease in WHSV while the selectivity of 2,4-DTBP increases with decreasing WHSV. This may be due to polyalkylation, enhanced by longer contact time and more availability of free alkylating agent. Based on phenol conversion as well as *p*-isomer (4-TBP) selectivity, WHSV of 4.86 h^{-1} was chosen as the optimum for further studies.

Figure 13 shows the effect of the n_{TBA}/n_{phenol} ratio on the phenol conversion and product selectivity over the FeSBA-1(36) catalyst at the reaction temperature of 200 °C and WHSV of 4.86 h^{-1}. It can be seen from Figure 13 that the phenol conversion increases from 54.2 to 78.5% with an increase in the n_{TBA}/n_{phenol} ratio from 1 to 3. The increase in phenol conversion with increasing n_{TBA}/n_{phenol} ratio may be attributed to a competition between the polar molecule TBA and phenol for adsorption sites. A similar result has also been found on the mono and bimetal substituted MCM-41 molecular sieves.[27,37] The low conversion at high n_{TBA}/n_{phenol} ratio may be due to the blocking of active sites by the adsorption of either the excess of *tert*-butanol or the water molecules produced from the dehydration of alcohol. This could also be attributed to slower diffusion rate of phenol because of a counter diffusion effect of *tert*-butanol and its products, and deactivation by oligomerization of excess olefin produced by the *tert*-butanol dehydration.

The sustainability of the catalysts in the *tert*-butylation of phenol was studied by carrying out the time on stream studies for duration of 6 h at 200 °C. An optimized n_{TBA}/n_{phenol} ratio of

1:3 and WHSV (4.86 h^{-1}) were maintained during the time on stream studies. The products were collected at a time interval of every 1 h. The phenol conversion over different catalysts during the time on stream study is presented in Figure 14.

The decrease in the conversion of phenol is marginal after several hours of time which indicates that FeSBA-1 catalyst does not deactivate quickly. Recently, Selvam and co-workers have found that the mesoporous catalysts with uni-dimensional pore system deactivates so quickly on the same reaction.[27] This indicates that the catalysts with three-dimensional pore system with very high surface area and specific pore volume are more effective in limiting the pore blocking due to deactivation than the catalysts with uni-dimensional pore system. The product selectivity over FeSBA-1(36) during time on stream is presented in Figure 15. Figure 15 shows that there is no appreciable change in selectivity of the products. The observed absence of deactivation are tentatively assigned to the three-dimensional pore structure of SBA-1, which limits pore blocking and allows a faster diffusion of the reactant molecules.[40-42]

Conclusions

In conclusion, our results reveal that Fe has been successfully incorporated for the first time into SBA-1 by simply adjusting the molar hydrochloric acid-to-surfactant ratio. The amount of Fe incorporation in SBA-1 can easily be controlled by the simple adjustment of the molar hydrochloric acid-to-silicon ratio. All the materials have been unambiguously characterized by AAS, XRD, N$_2$ adsorption, UV–Vis DRS, XPS, and ESR spectroscopy. The results from AAS, XRD, and N$_2$ adsorption reveal that the iron atom can be incorporated in the framework of SBA-1 matrix without altering the structural order and the

textural parameters. The nature and the coordination of iron atoms were extensively studied by XPS spectroscopy and found that most of the iron atoms in FeSBA-1 is in +3 coordination state. UV−Vis DRS and ESR studies confirm that the majority of the Fe atoms in FeSBA-1 exist in a tetrahedral coordination environment (most probably occupying framework positions). The catalytic activity of the novel catalyst was investigated in the vapor phase *tert*-butylation of phenol reaction. FeSBA-1(36) was found to be more active than previously studied systems such as FeAlMCM-41 or sulfated zirconia. The observed phenol conversion of 78.5% and selectivity toward 4-TBP of 70% is significantly higher as compared to other mono and bimetal substituted uni-dimensional MCM-41 molecular sieves under optimized reaction conditions.

References and Notes

(1) Kresge, C. T.; Leonowicz, M. E.; Roth, W. J.; Vartuli, J. C.; Beck, J. S. *Nature* **1992**, *359*, 710.

(2) Zhao, D.; Huo, Q.; Feng, J.; Chmelka, B. F.; Stucky, G. D. *J. Am. Chem. Soc.* **1998**, *120*, 6024.

(3) Hartmann, M.; Vinu, A. *Langmuir* **2002**, *18*, 8010.

(4) Vinu, A.; Murugesan, V.; Hartmann, M. *J. Phys. Chem. B.* **2004**, *108*, 7323.

(5) Vinu, A.; Murugesan, V.; Tangermann, O.; Hartmann, M. *Chem. Mater.* **2004**, *16*, 3056.

(6) Vinu, A.; Murugesan, V.; Böhlmann, W.; Hartmann, M. *J. Phys. Chem. B.* **2004**, *108*, 11496.

(7) Huo, Q.; Margolese, D. I.; Ciesla, U.; Feng, P.; Gier, T. E.; Sieger, P.; Leon, R.; Petroff, P. M.; Schüth, F.; Stucky, G. D. *Nature* **1994**, *368*, 317.

(8) Huo, Q.; Margolese, D. I.; Ciesla, U.; Demuth, D. G.; Feng, P.; Gier, T. E.; Sieger, P.; Firouzi, A.; Chmelka, B. F.; Schüth, F.; Stucky, G. D. *Chem. Mater.* **1994**, *6*, 1176.

(9) Huo, Q.; Leon, R.; Petroff, P. M.; Stucky, G. D. *Science* **1995**, *268*, 1324.

(10) Huo, Q.; Margolese, D. I.; Stucky, G. D. *Chem. Mater.* **1996**, *8*, 1147.

(11) Sakamoto, Y.; Kaneda, M.; Terasaki, O.; Zhao, D.; Kim, J. M.; Stucky, G. D.; Shin, H. J.; Ryoo, R. *Nature* **2000**, *408*, 449.

(12) Vinu, A.; Murugesan, V.; Hartmann, M. *Chem. Mater.* **2003**, *15*, 1385.

(13) (a) Dai, L.-X.; Tabata, K.; Suzuki, E.; Tatsumi, T. *Chem. Mater.* **2001**, *13*, 208. (b) Dai, L.-X.; Teng, Y.-H.; Tabata, K.; E. Suzuki, E.; Tatsumi, T. *Chem. Lett.* **2000**, 794.

(14) Che, S.; Sakamoto, Y.; Terasaki, O.; Tatsumi, T. *Chem. Mater.* **2001**, *13*, 2237.

(15) Hartmann, M.; Vinu, A.; Elangovan, S. P.; Murugesan, V.; Böhlmann, W. *Chem. Commun.* **2002**, *11*, 1238.

(16) Vinu, A.; Dedecek, J.; Murugesan, V.; Hartmann, M. *Chem. Mater.* **2002**, *14*, 2433.

(17) Chen, H.-Y.; Sachtler, W. M. H. *Catal. Today* **1998**, *42*, 73.

(18) Shilov, A. E.; Shulpin, G. B. *Chem. Rev.* **1997**, *97*, 2879.

(19) Valyon, J.; Millman, W. S.; Hall, W. K. *Catal. Lett.* **1994**, *24*, 215.

(20) Vinu, A.; Krithiga, T.; Murugesan, V.; Hartmann, M. *Adv. Mater.* **2004**, *16*, 1817.

(21) Knop, A.; Pilato, L. A. *Phenolic resin chemistry;* Springer: Berlin, 1985.

(22) Niederl, J. B.; Natelson, S. *J. Am. Chem. Soc.* **1938**, *53*, 272.

(23) Chandra, K. G.; Sharma, M. M. *Catal. Lett.* **1993**, *19*, 309.

(24) Parton, R. F.; Jacobs, J. M.; Huybrechts, D. R.; Jacobs, P. A. *Stud. Surf. Sci. Catal.* **1989**, *46*, 163.

(25) Parton, R. F.; Jacobs, J. M.; Ootehem, H. V.; Jacobs, P. A. *Stud. Surf. Sci. Catal.* **1989**, *46*, 211.

(26) Zhang, K.; Huang, C.; Zhang, H.; Xiang, S.; Liu, S.; Xu, D.; Li, H. *Appl. Catal. A: General* **1998**, *166*, 89.

(27) a) Sakthivel, A.; Badamali, S. K.; Selvam, P. *Microporous Mesoporous Mater.* **2000**, *39*, 457. (b) Badamali, S. K.; Sakthivel, A.; Selvam, P. *Catal. Lett.* **2000**, *65*, 153; c) Sakthivel, A.; Saritha, N.; Selvam, P. *Catal. Lett.* **2001**, *72*, 225.

(28) Kruk, M.; Jaroniec, M.; Sayari, A. *Langmuir* **1997**, *13*, 6267.

(29) Bordiga, S.; Buzzoni, R.; Geobalda, F.; Lamberti, C.; Giomello, E.; Zecchina, A.; Leofani, G.; Petrini, G.; Tozzola, G.; Vlaic, G. *J. Catal.* **1996**, *148*, 486.

(30) Wang, Y.; Zhang, Q.; Shishido, T.; Takehira, K. *J. Catal.* **2002**, *209*, 186.

(31) Moreno-Castilla, C.; Maldonado-Hodar, F. J.; Perez-Cadenas, A. F. *Langmuir* **2003**, *19*, 5650.

(32) Stakheev, A. Y.; Shpiro, E. S.; Apijok, J. *J. Phys. Chem.* **1993**, *97*, 5668.

(33) Reddy, E. P.; Davydov, L.; Smirniotis, P. G. *J. Phys. Chem B* **2002**, *106*, 3394.

(34) Wagner, C. D.; Riggs, W. M.; Davis, L. E.; Moulder, J. F.; Muilenberg, G. E. *Handbook of X-ray Photoelectron Spectroscopy;* Perkin-Elmer, Physical Electronics Division: Eden Prairier, MI, 1978.

(35) Tuel, A.; Acron, I.; Millet, J. M. M. *J. Chem. Soc., Faraday Trans. B* **1998**, *94*, 3501.

(36) (a) Goldfarb, D.; Bernardo, M.; Strohmaier, K. G.; Vaughan, D. E. W.; Thomann, H. *J. Am. Chem. Soc.* **1994**, *116*, 6344; b) Goldfarb, D.; Strohmaier, K. G.; Vaughan, D. E. W.; Thomann, H.; Poluetkov, O. G.; Schmidt, J. *J. Am. Chem. Soc.* **1996**, *118*, 4665.

(37) Vinu, A.; Usha Nandhini, K.; Murugesan, V.; Böhlmann, W.; Umamaheswari, V.; Pöppl, A.; Hartmann, M. *Appl. Catal., A* **2004**, *265*, 1.

(38) Deka, R. C.; Vetrivel, R. *J. Catal.* **1998**, *174*, 88.

(39) Song, C.; Ma, X.; Schmitz, A. D.; Schobert, H. H. *Appl. Catal., A* **1999**, *182*, 175.

(40) Dapurkar, S. E.; Selvam, P. *J. Catal.* **2004**, *224*, 178.

(41) Pu, S. B.; Kim, J. B.; Seno, M.; Inui, M. T. *Microporous Mater.* **1997**, *10*, 25.

(42) Dapurkar, S. E.; Selvam, P. *Appl. Catal. A* **2003**, *254*, 239.